Phase Evolution and Nature of Oxide Dissolution in Metallurgical Slags

Zhi H. I. Sun
Dept. of Metallurgy and Materials Engineering, KU Leuven, 3001 Leuven, Belgium

Xiaoling Guo, Joris Van Dyck, Muxing Guo, and Bart Blanpain
Dept. of Metallurgy and Materials Engineering, KU Leuven, 3001 Leuven, Belgium

DOI 10.1002/aic.14073
Published online March 15, 2013 in Wiley Online Library (wileyonlinelibrary.com)

The dissolution of solid lime particles into liquid slags at high temperatures was evaluated by means of confocal scanning laser microscopy. An additional solid layer around the lime particle was observed at the intermediate stage of the dissolution into CaO—Al_2O_3—SiO_2 slags. The dissolution rate was decelerated due to the existence of the additional layer and the dissolution profile could be clearly distinguished into three stages, that is, an early, intermediate, and late stage. By adding 10 wt % MgO, this layer could be effectively eliminated and the slope of the whole dissolution profile kept relatively constant. The dissolution path and mechanisms were subsequently evaluated by incorporating thermodynamic calculations. Both direct and indirect dissolutions could be distinguished. It was realized that the decrease in composition range for solid precipitating after adding MgO could significantly reduce the interfacial reaction (IR) layer formation. Post-mortem analyses on quenched samples were further carried out to confirm the theoretical calculations. It was found that the solid layer in slags without MgO was $(CaO)_2{\cdot}SiO_2$ and $(CaO)_3{\cdot}SiO_2$ which is in line with the thermodynamic calculations. However, only $(CaO)_2{\cdot}SiO_2$ was noticed in slags with MgO which both $(CaO)_2{\cdot}SiO_2$ and MgO phases should be present according to the calculations. The nonequilibrium during dissolution may play an important role on phase transformation and MgO particles in much smaller quantity may have dissolved into $(CaO)_2{\cdot}SiO_2$ phase. The diffusion of CaO in both slags with and without MgO was additionally investigated. The local CaO concentration distributions from the direct dissolution phase to the slag bulk could be well fitted with the theoretical model proposed via Fick's second law. As a result, the local diffusion coefficient in the dissolution region was obtained and the effect of MgO addition on diffusion could be assessed. © 2013 American Institute of Chemical Engineers *AIChE J*, 59: 2907–2916, 2013
Keywords: dissolution, confocal scanning laser microscopy, thermodynamic calculation, diffusion

Introduction

Dissolution, a process of dissolving solid or liquid into a solvent, is a ubiquitous phenomenon in the field of engineering. Decomposition of biomass,[1] leaching of mineral ores,[2] corrosion of refractory materials,[3] and dissolution of solid additives for impurity removal in ladle metallurgy[4] are only a few examples where a breakdown of the crystal lattice occurs forming a homogeneous mixture with the solvent. There are mainly two categories of dissolution, that is, direct and indirect.[5] During indirect dissolution, a firm product layer or non-flaking ash will be formed outside the particle while the whole solid particle size (including the product layer) remains unchanged. In this case, the process may include such steps as (1) diffusion of liquid reactant through the boundary layer (liquid film) surrounding the particle to the surface of the particle, (2) penetration and diffusion of liquid reactant through the layer of non-flaking ash, (3) chemical reaction at the interface between the non-flaking ash and the particle, and (4) diffusion of the products through the product layer and the boundary layer.[5] The dissolution can be rate limited by any of the steps or a combination. It can be influenced by various factors, for example, temperature, particle size, agitation conditions, and so on. Although the apparent kinetics can be readily obtained by characterizing the samples after dissolution, the real-time dissolution mechanism can be very complex and decisive conclusions on the dissolution mechanisms is difficult to be reached.[6] Direct dissolution is relatively faster and no ash/residue is formed outside the particle or the ash is flaking.[5]

In this research, lime is adopted to understand the dissolution mechanisms in CaO-based slags. The reason is that lime is very commonly used in many high temperature processes and its dissolution in slags is very representative. The dissolution nature is of broad interest and a better understanding of the lime dissolution in liquid slags will be helpful to chemical/metallurgical process design and optimization.

Lime is used in primary steelmaking, for example, basic oxygen furnace and electric arc furnace processes, where lime or dolomite is added as a fluxing additive to obtain a basic slag and help to remove harmful impurities such as sulfur and phosphorous.[7,8] Another process involving lime

Correspondence concerning this article should be addressed to Z. H. I. Sun at zhisun@126.com.

Current address of Z. H. I. Sun: School of Chemical Engineering, The University of Queensland, 4072 Brisbane, Australia.

dissolution is the entrained flow gasifier for power production, where lime is used as flux to lower the melting point of the coal ash slag.[9] The ash that remains after coal combustion typically contains SiO_2, CaO, Al_2O_3, and/or FeO.[9] The slag properties, for example, viscosity and refractory corrosion behavior, are associated with its evolution and slagging process where the lime dissolution is a key issue.[7,10–12] By increasing the lime addition, the resulting slag becomes less viscous and can be tapped from the base of the gasifier. In both cases, the rapid and complete dissolution of lime into the molten slag is very important to ensure its effective utilization. Calcium fluoride (fluorspar) has been known as an efficient flux which can enhance the lime dissolution[13,14] by increasing the diffusivity of CaO. However, owing to the emission of fluorine containing species into the atmosphere and potential contamination to the soil during slag disposal, the use of fluoride is limited.[15] Therefore, many efforts have been made to find alternative fluxes to replace fluorspar.[15–18] MnO_x, FeO_x, and TiO_2 are found to increase the lime dissolution[17] as the viscosity of the slag and CaO diffusivity are modified. SiO_2 is found to decrease the lime dissolution by increasing the viscosity.[19] In a $CaO—Al_2O_3—SiO_2$ slag, a layer of Ca_2SiO_4 can be found and the diffusion in this solid product tends to be of vital importance for the dissolution rate.[7] If the slag contains a sufficient amount of Fe_2O_3,[20] the product layer becomes discontinuous and it will be beneficial for the lime dissolution. To detect the dissolution mechanism, the most common method is the so-called "finger test" technique where a "rotating or static lime cylinder" is dipped into a molten ash/slag and exposed for a certain period.[11] After the test, the cylinder is taken out and characterized. The dissolution kinetics as well as the mechanisms can be obtained by analyzing the distribution of the phases through the cross-section of the sample. However, this method suffers as (1) intrinsically indirect determination and data may become questionable, especially when a discontinuous layer of solid phases are formed. In this case, it is difficult to determine the origination of the discontinuity (e.g., thin continuous layer could become discontinuous during quenching); (2) dissolution kinetics is influenced by the rotation rate during "finger test" and the real kinetics is difficult to be reflected; and (3) the samples may be easily broken up and the local situation becomes different which make it difficult to obtain conclusive results.[9,11,12,21,22]

Recently, high temperature confocal scanning laser microscopy (CSLM) has become available providing a direct observation of metallurgical phenomena at high temperatures.[23–25] Highlighted work with respect to the CSLM technique has been performed on various topics, such as inclusion behavior in metal melts,[26] phase transformations,[27] and also dissolution of oxide particles such as magnesia, alumina, zirconia, and spinel.[16,26,28] This technique not only provides an *in situ* observation, but also makes it possible to control the dissolution process online by adjusting the temperature or heating rate. Nevertheless, one of the limitations of the CSLM so far is that precise online phase/composition analysis is still under development. Traditionally, post-mortem analyses of quenched samples are combined with the *in situ* observation.[16,26] However, information about phase transformation may be lost, for example, precipitates of very small size are neglected, since the dissolution process is far from equilibrium. Conversely, instantaneous chemical reactions may still be possible during quenching and, therefore, some details of the dissolution can still be overlooked.

Table 1. Compositions (wt %) of the Slags Used in This Study

Slag Number	CaO	SiO_2	Al_2O_3	MgO	Basicity (CaO/SiO_2)
SM01	45.0	45.0	10.0	0	1.0
SM02	30.0	60.0	10.0	0	0.5
SM03	40.0	40.0	20.0	0	1.0
SM04	26.7	53.3	20.0	0	0.5
SM1	40.0	40.0	10.0	10.0	1.0
SM2	26.7	53.3	10.0	10.0	0.5
SM3	35.0	35.0	20.0	10.0	1.0
SM4	23.3	46.7	20.0	10.0	0.5

In this work, thermodynamic calculations are performed in accordance with the *in situ* observation and post-mortem analyses. This approach provides more reliable information on the dissolution nature of micrometer-sized lime particles into $CaO—Al_2O_3—SiO_2$-based slags. The information is obtained by concurrently characterizing (1) the phase transformation during dissolution, (2) the effect of MgO additive on dissolution, and (3) the evaluation of CaO diffusion through the boundary layer.

Materials and Experiments

Materials

The slags consisted of Al_2O_3, SiO_2, and CaO with or without MgO. They were prepared by blending the pure oxide compounds in a molybdenum crucible. Before mixing, all the oxides were dried in a muffle furnace at 300°C for 24 h. After obtaining a homogeneous mixture, the crucible was placed in a tube furnace under purified argon atmosphere and held for at least 24 h at a temperature of 1600°C. As soon as the premelting finished, the slags were quenched against a steel plate and crushed into small particles that were then remelted in the CSLM to release all the gases before running an experiment. The compositions of the pre-melted slags are listed in Table 1. The oxides used during the experiments were produced by Alfa Aesar, all with purities of 99.95 wt %. The lime particles for dissolution were also produced by Alfa Aesar and prepared from coarse lime grains. The fresh lime particles were always taken from the special container just before each dissolution experiment. Before dissolution, the particles were dried in a muffle furnace at 600°C for 24 h to remove water.

Experimental apparatus and procedures

The CSLM-IIF equipment (CSLM, Lasertec, 1LM21M-SVF17SP) was used to carry out *in situ* observations of lime dissolution at high temperature. A detailed description of the CSLM equipment can be found in our previous work.[6,29] The furnace chamber is gold-plated inside and ellipsoidal in shape. The crucible is placed in the upper focal point of the elliptical heating chamber and a halogen heating lamp is located in the lower focal point. The temperature is controlled by a B-type thermocouple welded at the bottom of the sample holder. HiTOS software contacting with a REX-P300 controller is used to program the temperature profiles. To ensure the accuracy of the measured temperature, thermocouple calibrations were performed using standard pure metal samples, for example, copper, nickel, and iron. A schematic view of the set up is given in Figure 1.

Before the dissolution experiments, the heating chamber was evacuated to ca. 10 Pa and refilled with ultra-purified argon gas for at least three times. The Ar gas had been passed

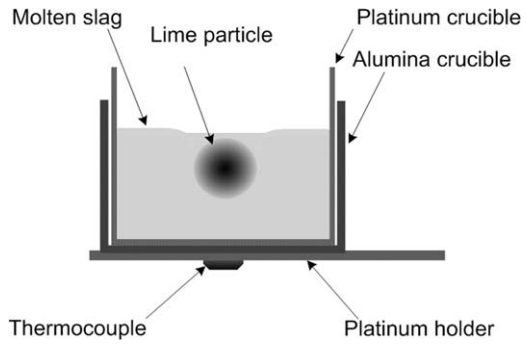

Figure 1. Schematic representation of the CSLM sample holder.

through a Restek triple filter and a Restek high capacity oxygen scrubber to remove oxygen, moisture, and hydrocarbons before being filled into the chamber. Then, the slag sample with a lime particle on the surface was heated to the desired temperature. The evaluation of the lime dissolution always started from the point where the set temperature was reached. To reduce the interaction of the slag and the particle before the slag melting, the sample was heated with a relatively high rate of around 200∼350°C/min. For each slag (Table 1), the dissolution experiments were performed at various temperatures.

In the present investigation, the lime particles were of irregular shape. To evaluate the changes of lime particle size during the dissolution, a border was constructed around the lime particle in the images obtained via the HiTOS software. An example is given in Figure 2 for the lime dissolution in slag SM1 at 1480°C. An equivalent radius was computed based on the measured area of the particle size. With the size evolution of the lime particle, the dissolution kinetics was derived.

Results and Discussion

In situ observation of lime dissolution in CAS-based slags

Figure 2 shows the lime dissolution process in slag SM1 at 1480°C. In each image, the boundary of the particle which is indicated by the dashed lines is extracted according to the image contrast. The particle which had an irregular shape becomes more spherical during dissolution. A rotation of the lime particle is also clearly noticeable in Figure 2 which results from the fluid flow due to a diffusional flux near the particle surface. During dissolution, this diffusional flux due to the change in the local radius of the particle when it is not spherical further results in compositional build-up.[6] The rotation introduces errors in the measurement of the particle size and probably influences the shape of the radius evolution profile. The dissolution process may, therefore, be affected by the rotation and local compositional build-up and the flow crossing the boundary layer between the particle and the slag bulk may be altered. The equivalent radius is calculated by assuming that the particle is a sphere and, therefore, the irregular shape of the particle is an important source of scatter in the dissolution profiles. Although this effect is important for the instantaneous measurement of particle size, the overall tendency of dissolution with time is not influenced, which is the essential information to determine dissolution mechanisms.

Interfacial reaction (IR) layer formation during lime dissolution in slags without MgO addition

In some experiments, a clear IR-layer structure could be observed during CaO dissolution, as shown in Figure 3 (indicated by arrows). The *in situ* observation showed that this layer formed after the CaO particle has been immersed into the molten slag for a certain time, suggesting an incubation period for its formation. The layer grew with time, reaching a maximum thickness. Afterwards, it dissolved into the slag, faded, and finally disappeared. The remaining lime then dissolved with a rapid rate. It has been found that the IR layer is more easily observed in slags without MgO addition and at lower temperatures. The formation of the IR layer influences directly the dissolution mechanisms and a lower dissolution rate is normally obtained.

Figure 4 gives the lime dissolution profile in slag SM04 at 1480°C. It can be found that the dissolution rate becomes very low from around 315 s indicating the formation of an IR layer. At both the early and late dissolution stages where

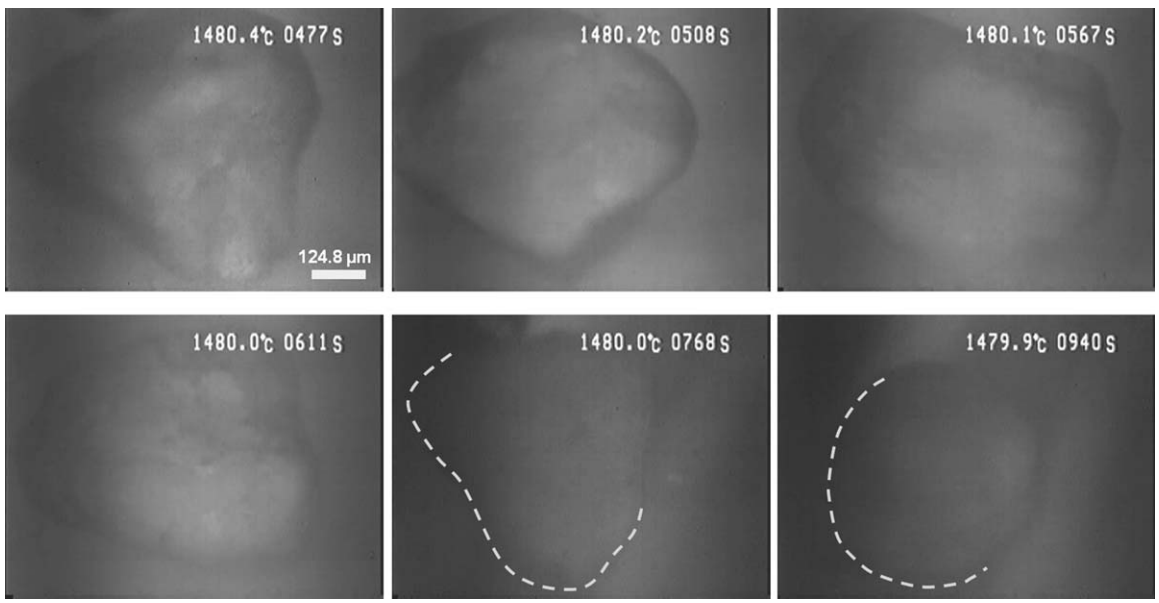

Figure 2. CSLM images of a slow CaO dissolution process in slag SM1 at 1480°C.

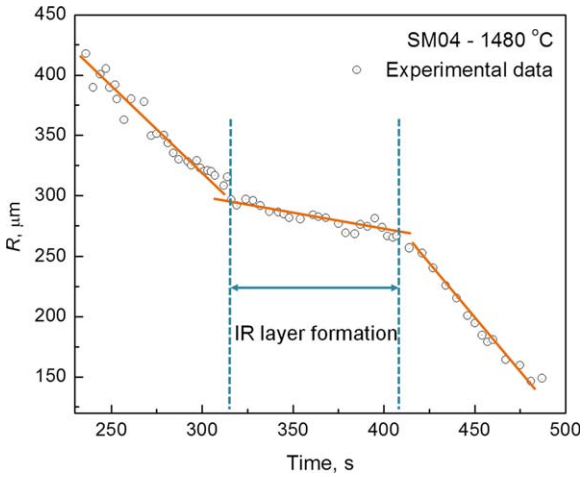

Figure 3. IR layer formed during CaO dissolved in slags without MgO: (a) slag SM02 (thinner layer) and (b) slag SM04 (thicker layer).

[Color figure can be viewed in the online issue, which is available at wileyonlinelibrary.com.]

no IR layer forms, the dissolution rates are significantly faster. It gives a direct proof that the IR-layer structure inhibits lime dissolution. Therefore, the current dissolution kinetics is intrinsically a multi-stage process and is influenced by a number of factors, for example, temperature, slag compositions, diffusional nature of CaO, and/or the local flow field. Those factors are apparently affecting the formation of the IR-layer structure.

In slags without MgO addition, it has been detected that temperature influences significantly the observation of an IR-layer structure with CSLM. This is reflected in the dissolution profiles. As shown in Figure 5, the IR layer formation range (with a lower dissolution rate) in the dissolution profile becomes much narrower with increasing the temperature. Since the lime particles were irregular and it was difficult to find two identical particles, the normalized particle size R/R_0 is provided in Figure 5a with R_0 the particle equivalent radius when the particle was just immerged in the slag which is corresponding to the starting time t_0 of the dissolution. At a sufficiently high temperature, for example, 1600°C, although the IR layer was still observed, it diminished rapidly. Figure 5b provides the corresponding images of different stages and the lower dissolution rate in the intermediate stage of dissolution can be clearly correlated to the IR-layer formation.

By adding MgO, the formation of IR-layer structure is found to be effectively prohibited. As shown in Figure 2, only one clear border of liquid slag-solid in the images is distinguished during dissolution. Figure 6 shows the lime dissolution profiles in slag SM1 at different temperatures. The dissolution rate which is reflected by the slope of the dissolution profile increases dramatically with temperature. Although a minor change of the slope during dissolution can still be observed, there is no clear transition region distinguishable comparing with Figure 5. The distinctive phenomena in slags with and without MgO addition can originate from the difference in their dissolution nature.

Dissolution path and phase identification

Dissolution Path. To understand the formation of the IR layer, the phase diagrams of the slag systems were calculated by using FactSage software with the FToxid database.[30] During dissolution, a concentration gradient of CaO is built between the bulk (liquid slag) and the lime particle. The dissolution path of CaO at a certain temperature and in a given slag passes through different phase zones in the phase diagrams. Although the dissolution is a nonequilibrium process and the dissolution path does not have to be a straight line, the phases which may precipitate adjacent to the particle can still be predicted by the phase diagrams. Figure 7 shows the phase diagrams of slags with and without MgO addition at 1600°C. The dissolution should stop at the CaO content, where the CaO monoxide phase starts to precipitate in the phase diagram. During dissolution of a lime particle, compositional gradient, for example, the content of CaO, from the lime particle to the slag bulk is expected. According to Figure 7, solid phase is precipitating at higher local CaO content between the lime particle and the slag. The freshly precipitated solid phase is further dissolved by the liquid slag and diffusion/transfer of CaO or Ca^{2+} should be associated. The accumulation/growth of the solid precipitates and observation of a clear IR layer with CSLM depends directly on the balance between precipitation and dissolution of the fresh solid phases and the CaO content range for solid phase precipitation becomes important.

In the case of slag SM02 (Figure 7a), dissolution stops at the composition of around ~72 wt % CaO and solid phase

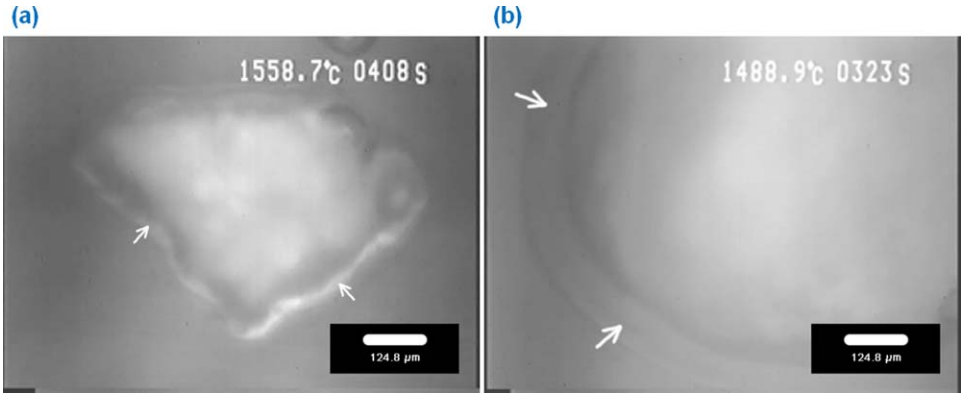

Figure 4. Lime dissolution profile in slag SM04 at 1480°C (*R*: the equivalent particle radius; straight lines are linear fitting of each dissolution stage).

A clear platform is observed due to the IR layer formation during dissolution. [Color figure can be viewed in the online issue, which is available at wileyonlinelibrary.com.]

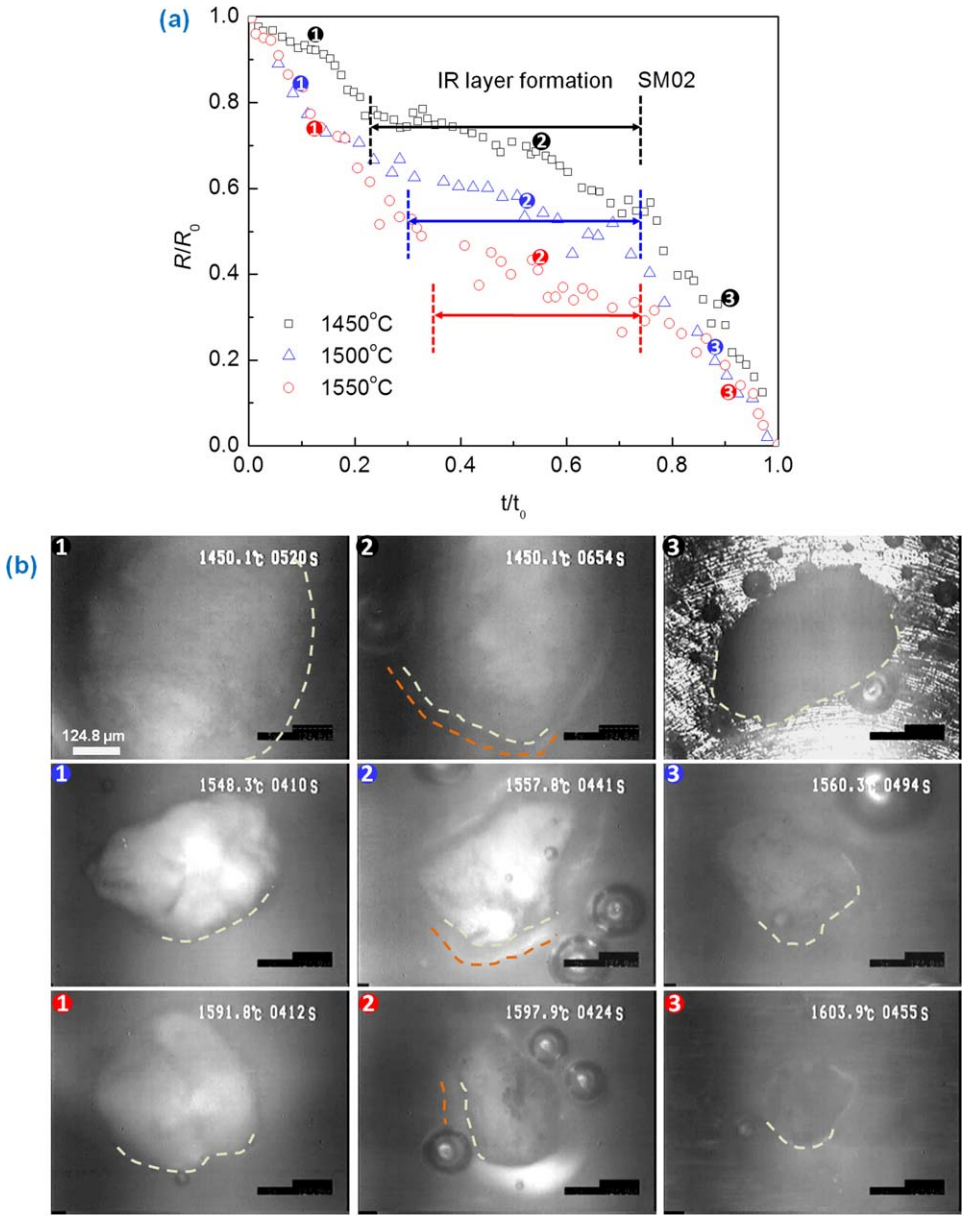

Figure 5. Lime dissolution profiles in slag SM02 without MgO addition at different temperatures.

(a) IR layer formation range becomes shorter with increasing temperature and (b) images of lime particles during dissolution at different stages. [Color figure can be viewed in the online issue, which is available at wileyonlinelibrary.com.]

starts to precipitate at ~52 wt % CaO. With the accumulation of CaO content in the slag during lime dissolution, two solid phases, that is, $(CaO)_2{\cdot}SiO_2$ and $(CaO)_3{\cdot}SiO_2$ will precipitate adjacent to the particle according to Figure 7a. The large CaO content range for solid phase precipitation (20 wt %) is believed important in forming the continuous solid layer or the IR-layer structure according to the *in situ* observation (Figure 3).

The IR layer contributes a lower dissolution rate after the dissolution proceeds a certain time (Figure 5). At the early stage, CaO dissolves directly into the liquid slag inducing a local compositional accumulation and it continues to diffuse into the bulk slag. The direct dissolution reaction can be given as

$$\mathrm{CaO(s)} \rightarrow (\mathrm{CaO}) \tag{1}$$

where small bracket () indicates the species in liquid slag.

When the precipitation of solid phases is promoted and a solid layer is formed, lime dissolution becomes indirect and the following reactions become thermodynamically important

$$3(\mathrm{CaO}) + (\mathrm{SiO_2}) \rightarrow (\mathrm{CaO})_3 \cdot \mathrm{SiO_2(s)} \tag{2}$$

$$2(\mathrm{CaO})_3 \cdot \mathrm{SiO_2(s)} + (\mathrm{SiO_2}) \rightarrow 3(\mathrm{CaO})_2 \cdot \mathrm{SiO_2(s)} \tag{3}$$

and/or

$$2(\mathrm{CaO}) + (\mathrm{SiO_2}) \rightarrow (\mathrm{CaO})_2 \cdot \mathrm{SiO_2(s)} \tag{4}$$

$$(\mathrm{CaO})_2 \cdot \mathrm{SiO_2(s)} \rightarrow 2(\mathrm{Ca^{2+}}) + (\mathrm{Si^{4+}}) + 4(\mathrm{O^{2-}}) \tag{5}$$

When the slag contains MgO, for example, SM2, the primary solid precipitate is $(CaO)_2{\cdot}SiO_2$ from the liquid slag when CaO content is relatively lower (e.g., at ~56 wt %) according to Figure 7b. Solid MgO phase is also

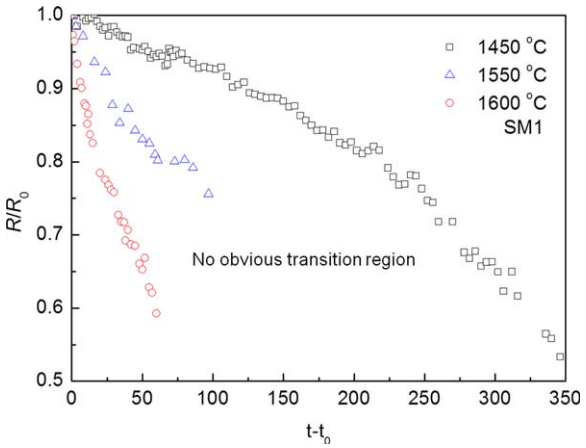

Figure 6. Lime dissolution profiles in slag SM1 with 10 wt. % MgO addition at different temperatures.

No obvious transition region can be distinguished. [Color figure can be viewed in the online issue, which is available at wileyonlinelibrary.com.]

precipitating together with $(CaO)_2{\cdot}SiO_2$, when the CaO is locally accumulating in the slag and the amount of MgO is much smaller. The CaO content for $(CaO)_2{\cdot}SiO_2$ precipitate ranges from ~56 to ~65 wt %. This small compositional range (9 wt %) may dramatically decrease the amount of $(CaO)_2{\cdot}SiO_2$ accumulation and the solid phase can be easily redissolved by the liquid slag comparing with slag SM02 (Figure 7a). Therefore, no IR layer was clearly observed under CSLM and the dissolution rate stayed nearly constant as shown in Figure 6. The dissolution is then following reactions (1), (4), and (5). If MgO crystals with large particle size are formed, the dissolution mechanisms may become more complex and spinel phase may be observed.[6]

Microstructural Characteristics at Lime Particle/Liquid Slag Interface. To verify the dissolution paths and reactions, a sample with IR-layer formation was quenched 1 s after the layer was clearly distinguished. It needs to be indicated that the formation of the IR layer is very rapid. The time is around 2–3 s from the first sight to a clear view of the layer. The sample with MgO addition was quenched 1 s after the particle is fully immerged into the slag. Figure 8 shows the secondary electron images of lime dissolving into slags SM02 and SM2 as well as their energy-dispersed X-ray (EDX) mappings. A single sharp edge is observed between the lime particle and the slag bulk for slag SM2 (Figure 8a), whereas an IR layer with CaO accumulation can be clearly distinguished for slag SM02 (Figure 8b). The layer exhibits compositional gradient from the particle to the slag bulk. It gives a direct proof that a solid layer is formed during lime dissolution in slags without MgO addition.

The compositions of different phases formed during dissolution were further analyzed. The morphologies of the phases are shown in Figure 9. For slag SM02, the experimental results correspond well with the phase diagram predictions (Table 2). Both $(CaO)_2{\cdot}SiO_2$ and $(CaO)_3{\cdot}SiO_2$ were found and $(CaO)_3{\cdot}SiO_2$ generates near to the lime particle. This is in agreement with the dissolution path given in Figure 7a (the dash line indicates the phase evolution from the liquid slag to periphery of the lime particle). However, the layer of $(CaO)_3{\cdot}SiO_2$ is very thin (<5 μm) and it is replaced immediately by $(CaO)_2{\cdot}SiO_2$ when CaO content becomes lower in the surrounding liquid slag (or when the location is sufficiently far from the particle). The $(CaO)_2{\cdot}SiO_2$ layer is found to be ~30 μm and continuous. This thickness was obtained when the solid layer started to be clearly distinguished. It had been realized that the solid layers formed in a very short time as mentioned above. Before the IR solid layer was formed, CaO diffusion/direct dissolution into the slag prevailed the dissolution process.

In slag SM2, a precipitate layer of ~5 μm is realized near to the lime particle (Figure 9a). The layer is discontinuous and contains a set of $(CaO)_2{\cdot}SiO_2$ crystals with a small amount of MgO (the compositions are shown in Table 2, C and C*). No pure MgO crystals were found in the sample which should precipitate together with $(CaO)_2{\cdot}SiO_2$ according to the phase diagram (Figure 7b). Slag SM2 is a quaternary system and Figure 7b is a projection of $CaO{-}SiO_2{-}Al_2O_3{-}MgO$ system to the ternary phase diagram. The representation of the dissolution/reaction path is not straightforward by Figure 7. However, the absence of MgO particles may be related to two reasons, that is,

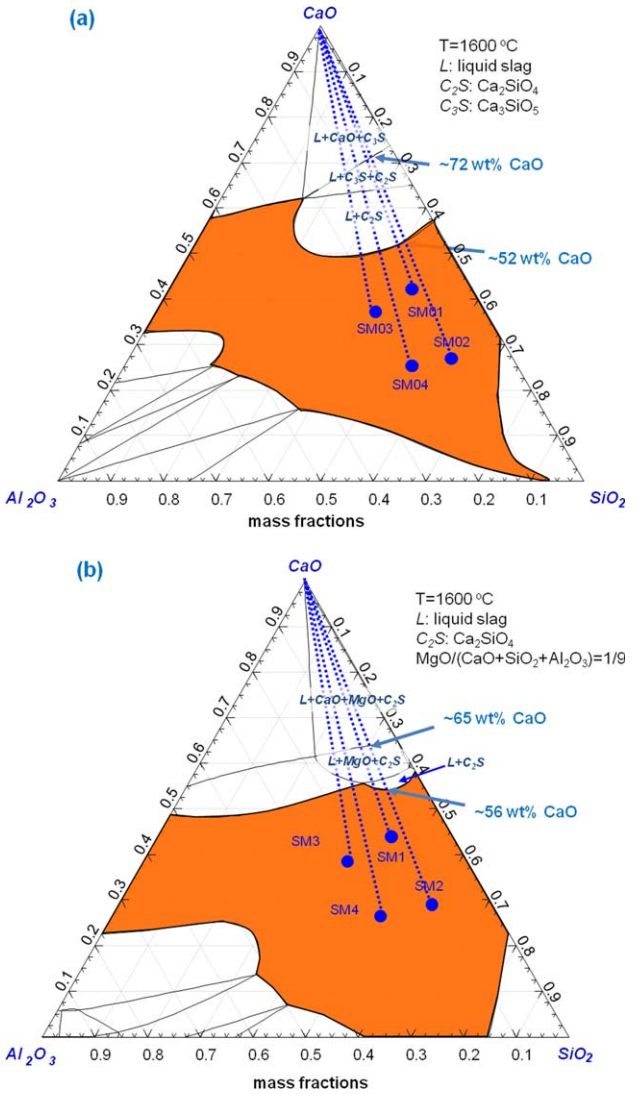

Figure 7. Phase diagrams of the slags in the present research.

(a) Slags without MgO addition and (b) slags with MgO addition. The direct dissolution paths for each slag are shown by the dash lines. [Color figure can be viewed in the online issue, which is available at wileyonlinelibrary.com.]

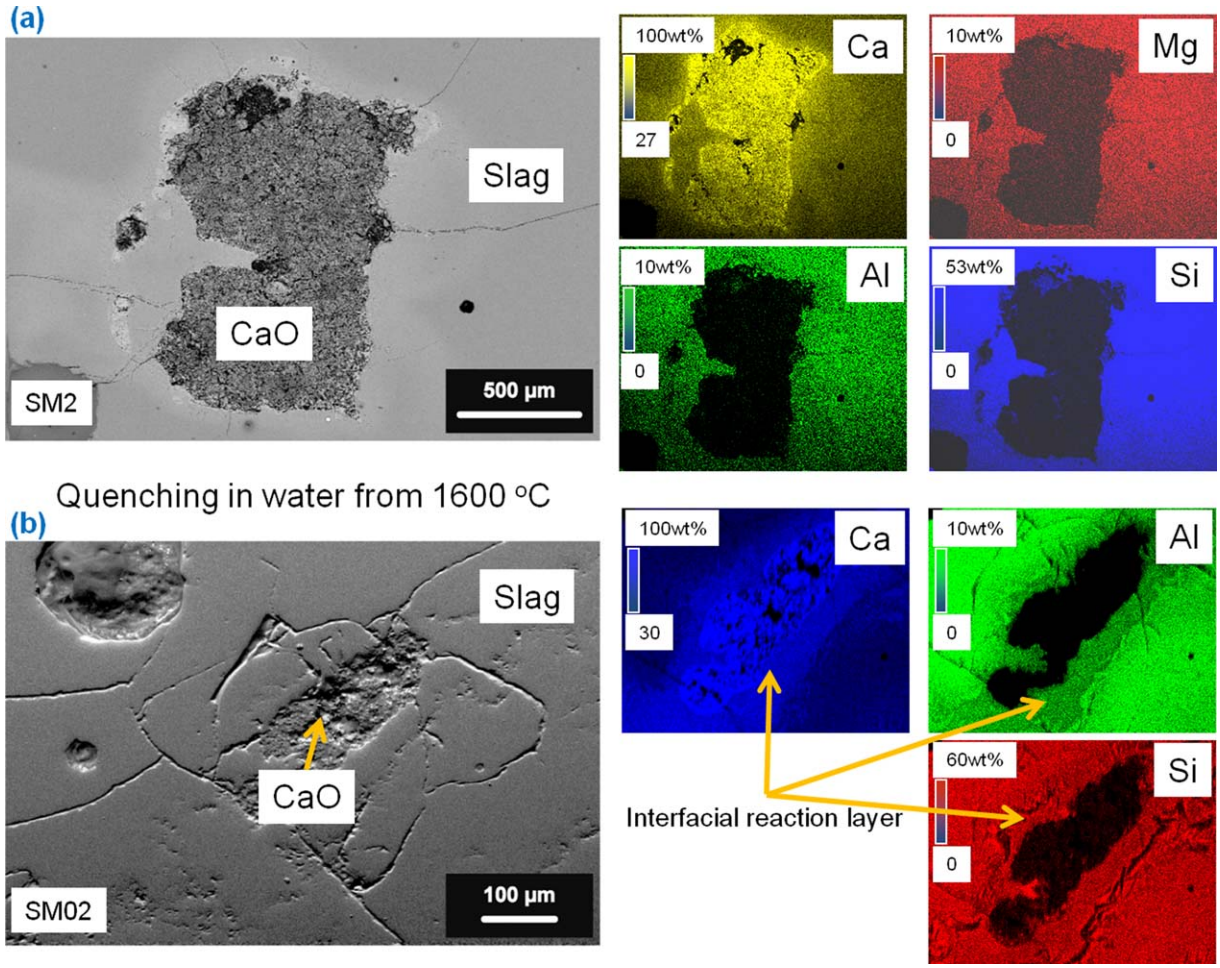

Figure 8. SEM images of lime particle dissolving into slags with (a) and without (b) MgO addition.

Energy-dispersed X-ray mappings indicates the distribution of the corresponding elements around the lime particles. [Color figure can be viewed in the online issue, which is available at wileyonlinelibrary.com.]

1. The fresh MgO crystals were too small to be detected with SEM.
2. MgO and $(CaO)_2{\cdot}SiO_2$ precipitate at the same time; since MgO is present in a relatively small concentration, it may form solid solution with $(CaO)_2{\cdot}SiO_2$ crystals (hypothetically).

According to the C and C* compositions in Table 2, the crystals can also be considered as Merwinite phase. However, it is difficult to draw this conclusion since the process is far from equilibrium. The precipitation of new phases may cause a compositional divergence in the slag from its original composition and result in depleted zones of SiO_2, Al_2O_3, and/or MgO. The shortage of these elements may be suppressed quickly if the required mass transport condition is fulfilled. Otherwise, the formation of new precipitates is interrupted and distinct phases may also be generated. Therefore, a detailed experimental verification on phase equilibria may be required to determine the exact phases.

In the present research, however, the kinetics and dissolution path are considered. Although the above analyses are not fully quantitative, they have already provided significant information to distinguish the effect of MgO on lime dissolution into liquid slags. On one aspect, the narrower CaO content range for solid precipitates in slags with MgO (Figure 7) addition initiates less solid precipitates and the solid layer becomes less visible under CSLM. On the other aspect, the layer of precipitates is discontinuous in slags with MgO (Figure 9a) and it can be easily redissolved into the liquid slags with lower CaO content. It indicates that MgO plays an important role in accelerating lime dissolution into liquid slags.

Effect of MgO on Lime Dissolution—Early Stage of the Dissolution. During lime dissolution, the diffusion of CaO into the slag through the product layer (direct dissolution phase, e.g., the thick layer in slag without MgO and the thin layer in slag with MgO, Figure 9) is of significant importance. The diffusion depends directly on the local slag compositions/properties and bears complex nature. In the traditional rotating lime cylinder experiments, the dissolution of lime can be highly influenced by the rotating speed which

Table 2. Composition of Different Phases Measured with Energy Dispersed X-Ray (EDX)

	NO.	Ca at %	Si at %	Al at %	Mg at %	Phases
SM2	A	50.75	0.98	0.18	0.29	CaO
	B	12.31	21.99	4.61	3.69	Liquid slag SM2
	C	26.36	16.81	1.04	5.92	C_2S + MgO
	C*	32.01	17.84	0.84	4.74	C_2S + MgO
SM02	D	48.51	0.73	0.29	–	CaO
	E	14.35	25.19	4.71	–	Liquid slag SM02
	F	24.53	16.60	0.23	–	C_2S layer
	G	46.24	17.10	0.15	–	C_3S

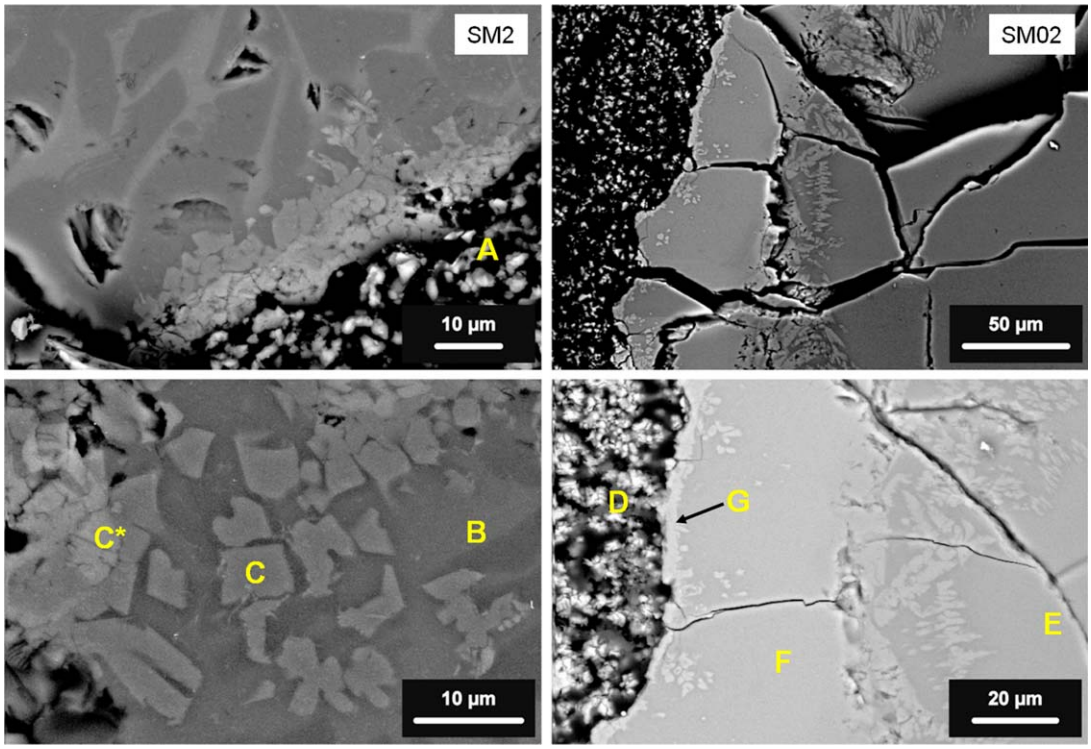

Figure 9. SEM images of different phases forming during lime particle dissolving into slags with (a) SM2 and without (b) SM02 MgO addition.

[Color figure can be viewed in the online issue, which is available at wileyonlinelibrary.com.]

may generate different flow patterns in different slags.[11] In the present case, the dissolution occurs at a relative quiescent condition although the rotation of lime particle induces deviation in the dissolution profile. The diffusion of CaO in the two types of slags can be compared by considering the CaO concentration profiles around the dissolution phases. As shown in Figure 10, the open circles indicate the CaO concentration profiles along the orange lines in the SEM images measured via EDX for the quenched samples. As indicated previously, the diffusion time for both samples is considered to be 1 s. In this case, the diffusion distance in slag SM2 (Figure 10b) is evidently longer than in slag SM02 (Figure 10b).

To reach a better understanding of the CaO diffusion, theoretical calculations were carried out according to Fick's second law. The relationship between the diffusion time and distance is expressed by[31]

$$\frac{\partial c_{\mathrm{CaO}}}{\partial t} = D_{\mathrm{CaO}} \frac{\partial^2 c_{\mathrm{CaO}}}{\partial x^2} \tag{6}$$

where D_{CaO} is the on-site diffusion coefficient of CaO, c_{CaO} is the concentration of CaO, t is the time, and x is the distance.

The diffusion coefficient D_{CaO} is associated with the slag properties by Stokes–Einstein equation[32]

$$D_{\mathrm{CaO}} = \frac{k_{\mathrm{B}} T}{6\pi r \eta} \tag{7}$$

where k_{B} is the Boltzmann constant, T is the temperature in K, η is the slag viscosity, and r is the effective molecules radius.

Since the local composition is different from the slag bulk and the viscosity may be increased due to the present of solid precipitates near to the direct dissolution phase (IR layer for SM02 and lime particle for SM2), the diffusion coefficient may also be modified and a lower D_{CaO} is expected than in the slag bulk. Therefore, the diffusion coefficient estimated by traditional approaches (apparent diffusion coefficient in a full liquid slag)[33] cannot be directly applied to the present calculations.

To facilitate the calculations, boundary conditions are chosen according to the experimental measurements in Figure 10 which may be different from the starting compositions of the slags in Table 1. The boundary conditions are as follows:

1. When at x_0 with the starting of CaO diffusion, c_{CaO} equals to the CaO content in the direct dissolution phase. For slag SM02, $x_0 = 32.5$ μm and $c^0{}_{\mathrm{CaO}} = 51.4$ wt % (Figure 10a); for slag SM2, $x_0 = 9.89$ μm and $c^0{}_{\mathrm{CaO}} = 85.6$ wt % (Figure 10b).
2. When x is significantly large or infinite, c_{CaO} equals the measured composition of the slag. For slag SM02, $c^s{}_{\mathrm{CaO}}$ is taken as 35.6 wt % (Figure 10a) and for slag SM2, $c^s{}_{\mathrm{CaO}}$ is taken as 45.6 wt % (Figure 10b).

The solutions of Eq. 6 under the above boundary conditions can be expressed as

$$\frac{c_{\mathrm{CaO}} - c^s{}_{\mathrm{CaO}}}{c^0{}_{\mathrm{CaO}} - c^s{}_{\mathrm{CaO}}} = \mathrm{erf}\left(\frac{x}{2\sqrt{D^{(0)}_{\mathrm{CaO}} t}}\right) \quad \text{for slag without MgO addition} \tag{8}$$

$$\frac{c_{\mathrm{CaO}} - c^s{}_{\mathrm{CaO}}}{c^0{}_{\mathrm{CaO}} - c^s{}_{\mathrm{CaO}}} = \mathrm{erf}\left(\frac{x}{2\sqrt{D^{(10)}_{\mathrm{CaO}} t}}\right) \quad \text{for slag with 10 wt \% MgO addition} \tag{9}$$

To reach the best fitting to the experimental measurement in the diffusion region, CaO concentration profiles were

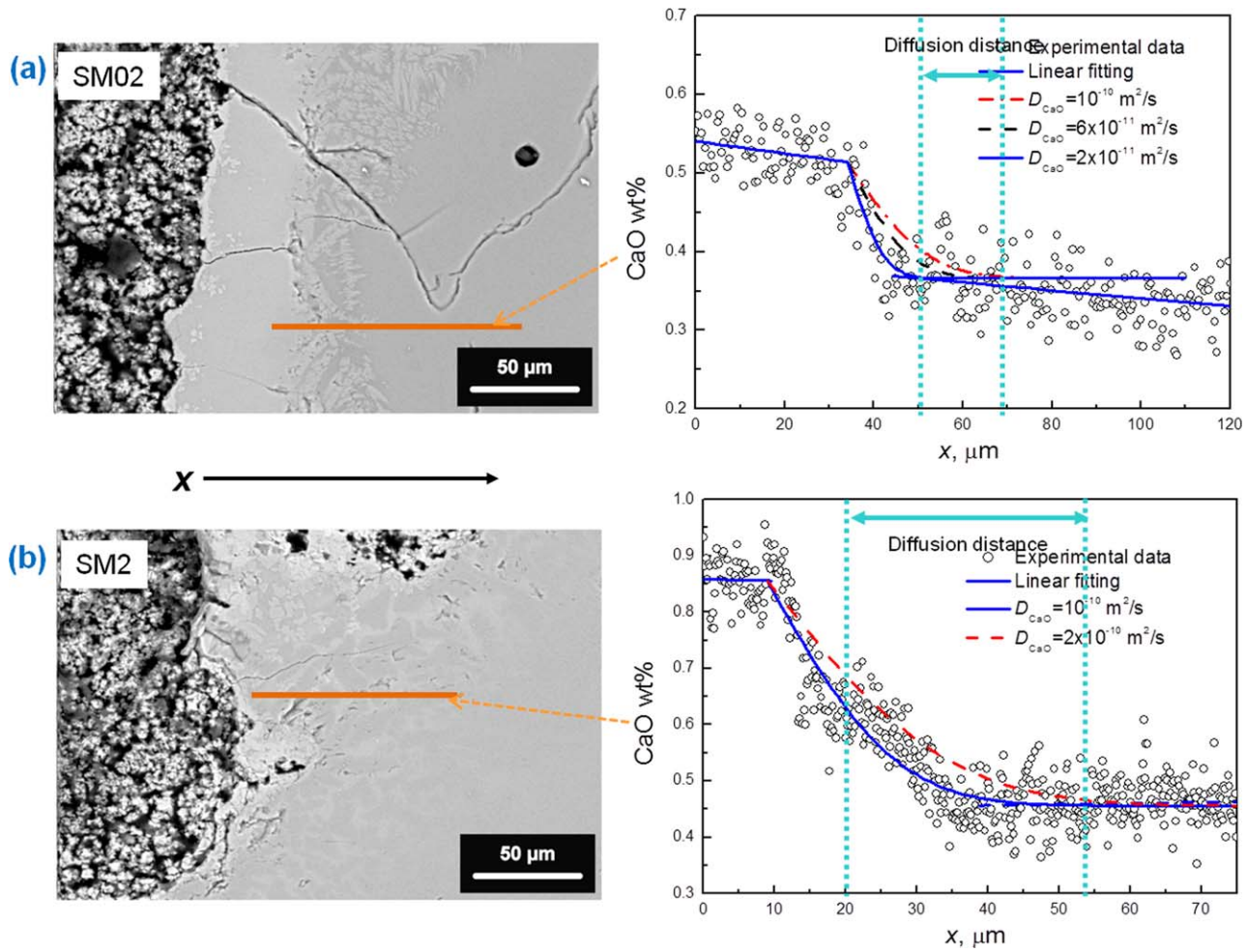

Figure 10. Line analyses of CaO distribution around the direct dissolution phases into slags SM02 (a) and SM2 (b) at 1600°C (orange lines are the measuring lines).

[Color figure can be viewed in the online issue, which is available at wileyonlinelibrary.com.]

calculated with different diffusion coefficient values by using Eqs. 8 and 9. The calculation results indicate that $D_{CaO}^{(0)} = 2 \times 10^{-11}$ m^2/s for slag SM02 and $D_{CaO}^{(10)} = 1 \times 10^{-10}$ m^2/s for slag SM2 at 1600°C gives the optimum fitting (Figure 10). It means that the diffusion in liquid slag without MgO addition is evidently slower than in slag with MgO addition. According to Eq. 7, the local diffusion coefficient is directly influenced by the local viscosity of the liquid slags. This has been highlighted that the addition of monoxides can break down silica networks in liquid slags[34] and the corresponding viscosity becomes lower. The addition of MgO contributes not only to get rid of the IR layer, but also to increase the diffusion rate and improve the kinetic conditions during lime dissolution in liquid slags. Beyond the results, the calculations provide a potential method to calculate the local diffusion coefficient combining with CSLM observation.

Conclusions

The dissolution of CaO particles in CaO—Al_2O_3—SiO_2-based slags with and without MgO has been investigated by using a CSLM and thermodynamic calculations between 1450°C and 1600°C. The conclusions can be drawn as:

1. The effect of MgO addition on lime dissolution has been discussed. Without MgO addition, the dissolution rate was decelerated due to the formation of an IR layer in slags and the dissolution profile could be clearly divided into three stages, that is, the early, intermediate, and late stages. The smallest dissolution rate, that is, slope of dissolution profile, is found at the intermediate stage of the dissolution. This implies that the IR layer forms when the local CaO accumulation becomes large enough. By adding 10 wt % MgO, this IR layer could be effectively gotten rid of and the slope of the whole dissolution profile then kept relatively constant.

2. Thermodynamic calculations are performed with FactSage software to evaluate the dissolution path and mechanisms. Both direct (CaO reacts with liquid slag) and indirect (through intermediate phase e.g., $(CaO)_2{\cdot}SiO_2$) dissolutions could take place under the certain experimental conditions. It was realized that the narrower CaO content range for solid phases in slags with MgO (Figure 7) addition initiates less solid precipitates and the solid layer becomes less visible under CSLM. On the other aspect, the layer of precipitates is discontinuous in slags with MgO (Figure 9a) and it can be easily redissolved into the liquid slags with lower CaO content.

3. Post-mortem analyses on quenched CSLM samples substantiate that the solid layer in slags without MgO are $(CaO)_2{\cdot}SiO_2$ and $(CaO)_3{\cdot}SiO_2$ which is in agreement with the thermodynamic calculations. Meanwhile, only $(CaO)_2{\cdot}SiO_2$ is detected in slags with MgO addition, whereas both $(CaO)_2{\cdot}SiO_2$ and MgO phases should be found

according to the calculations. This disagreement between thermodynamic calculations and post-mortem analyses is believed to be caused by the nonequilibrium between different phases during dissolution and MgO particles in small quantity may dissolve into $(CaO)_2{\cdot}SiO_2$ phase forming a solid solution.

4. Theoretical calculations are performed to assess the diffusion of CaO in both slags with and without MgO. The local diffusion coefficient in the dissolution region is obtained by fitting the experimental data and the calculated results. It has been estimated that the local diffusion coefficient $D_{CaO}^{(0)} = 2 \times 10^{-11}$ m^2/s for slag SM02, whereas $D_{CaO}^{(10)} = 1 \times 10^{-10}$ m^2/s for slag SM2 at 1600°C. The addition of MgO can significantly increase the diffusion coefficient and improve kinetics of lime dissolution into liquid slags.

Literature Cited

1. Becidan M, Várhegyi G, Hustad JE, Skreiberg Ø. Thermal decomposition of biomass wastes. A kinetic study. *Ind Eng Chem Res*. 2007;46:2428–2437.
2. Sun Z, Zhang Y, Zheng S-L, Zhang Y. A new method of potassium chromate production from chromite and KOH-KNO_3-H_2O binary submolten salt system. *AIChE J*. 2009;55:2646–2656.
3. Guo M, Jones PT, Parada S, Boydens E, Dyck JV, Blanpain B, Wollants P. Degradation mechanisms of magnesia-chromite refractories by high-alumina stainless steel slags under vacuum conditions. *J Eur Ceram Soc*. 2006;26:3831–3843.
4. Valdez M, Prapakorn K, Cramb AW, Sridhar S. Dissolution of alumina particles in CaO-Al_2O_3-SiO_2-MgO slags. *Ironmak Steelmak*. 2002;29:47–52.
5. Levenspiel O. Chemical Reaction Engineering, 3rd ed. New York: John Wiley & Sons, 1999.
6. Liu J, Guo M, Jones PT, Verhaeghe F, Blanpain B, Wollants P. In situ observation of the direct and indirect dissolution of MgO particles in CaO-Al_2O_3-SiO_2-based slags. *J Eur Ceram Soc*. 2007;27:1961–1972.
7. Yang J, Kuwabara M, Asano T, Chuma A, Du J. Effect of lime particle size on melting behavior of lime-containing flux. *ISIJ Int*. 2007;47:1401–1408.
8. Fruehan R. Desulfurization of liquid steel containing aluminum or silicon with lime. *Metall Mater Trans B*. 1978;9:287–292.
9. Elliott LK, Lucas JA, Happ J, Patterson J, Hurst H, Wall TF. Rate limitations of lime dissolution into coal ash slag. *Energy Fuels*. 2008;22:3626–3630.
10. Lee WE, Zhang S. Melt corrosion of oxide and oxide-carbon refractories. *Int Mater Rev*. 1999;44:77–104.
11. Elliott L, Wang SM, Wall T, et al. Dissolution of lime into synthetic coal ash slags. *Fuel Process Technol*. 1998;56:45–53.
12. Deng T, Gran J, Sichen D. Dissolution of lime in synthetic FeO-SiO_2 and CaO-FeO-SiO_2 slags. *Steel Res Int*. 2010;81:347–355.
13. Kor G. Effect of fluorspar and other fluxes on slag-metal equilibria involving phosphorus and sulfur. *Metall Mater Trans B*. 1977;8:107–113.
14. Wang H, Li G, Ren Z, Li B, Zhang X, Shi G. LATS refining ladle slag modifying with CaO-CaF_2. *J Univ Sci Technol Beijing*. 2007;14:125–129.
15. Fox AB, Mills KC, Lever D, et al. Development of fluoride-free fluxes for billet casting. *ISIJ Int*. 2005;45:1051–1058.
16. Fox AB, Valdez ME, Gisby J, Atwood RC, Lee PD, Sridhar S. Dissolution of ZrO_2, Al_2O_3, MgO and $MgAl_2O_4$ particles in a B_2O_3 containing commercial fluoride-free mould slag. *ISIJ Int*. 2004;44:836–845.
17. Amini S, Brungs M, Ostrovski O, Jahanshani S. Effects of additives and temperature on dissolution rate and diffusivity of lime in Al_2O_3-CaO-SiO_2 based slags. *Metall Mater Trans B*. 2006;37:773–780.
18. Wen GH, Sridhar S, Tang P, Qi X, Liu YQ. Development of fluoride-free mold powders for peritectic steel slab casting. *ISIJ Int*. 2007;47:1117–1125.
19. Kondratiev A, Jak E, Hayes P. Predicting slag viscosities in metallurgical systems. *JOM—J Min Met Mat Soc*. 2002;54:41–45.
20. Amini SH, Brungs MP, Jahanshahi S, Ostrovski O. Effects of additives and temperature on dissolution rate and diffusivity of lime in Al_2O_3-CaO-SiO_2 based slags. *Metall Mater Trans B—Proc Metall Mater Proc Sci*. 2006;37:773–780.
21. Satyoko Y, Lee WE, Parry E, Richards P, Houldsworth IG. Dissolution of iron oxide containing doloma in model basic oxygen furnace slag. *Ironmak Steelmak*. 2003;30:203–208.
22. Orrling C, Sridhar S, Cramb AW. In situ observation of the role of alumina particles on the crystallization behavior of slags. *ISIJ Int*. 2000;40:877–885.
23. Yin HB, Shibata H, Emi T, Suzuki M. In-situ observation of collision, agglomeration and cluster formation of alumina inclusion particles on steel melts. *ISIJ Int*. 1997;37:936–945.
24. Soll-Morris H, Sawyer C, Zhang ZT, Shannon GN, Nakano J, Sridhar S. The interaction of spherical Al_2O_3 particles with molten Al_2O_3-CaO-FeOx-SiO_2 slags. *Fuel*. 2009;88:670–682.
25. Zhang P, Debroy T, Seetharaman S. Interdiffusion in the MgO-Al_2O_3 spinel with or without some dopants. *Metall Mater Trans A*. 1996;27:2105–2114.
26. Lee SH, Tse C, Yi KW, Misra P, Chevrier V, Orrling C, Sridhar S, Cramb AW. Separation and dissolution of Al_2O_3 inclusions at slag/metal interfaces. *J Non-Cryst Solids*. 2001;282:41–48.
27. Kim JH, Kim SG, Inoue A. In situ observation of solidification behavior in undercooled Pd-Cu-Ni-P alloy by using a confocal scanning laser microscope. *Acta Mater*. 2001;49:615–622.
28. Liu J, Verhaeghe F, Guo M, Blanpain B, Wollants P. In situ observation of the dissolution of spherical alumina particles in CaO-Al_2O_3-SiO_2 melts. *J Am Ceram Soc*. 2007;90:3818–3824.
29. Guo X, Guo M, Sun Z, Van Dyck J, Blanpain B, Wollants P. Chemical dissolution of lime particles in CaO-Al_2O_3-SiO_2-based slags: an in situ observation approach. Materials Science and Technology (MS&T) 2010 Conference and Exhibition, October 17–21, 2010:1739–1750.
30. FactSage version 6.3. July 26, 2012. Available at: http://www.factsage.com/
31. Poirier DR, Geiger GH. Transport Phenomena in Materials Processing. Warrendale: TMS, 1994.
32. Kooijman HA. A modification of the Stokes–Einstein equation for diffusivities in dilute binary mixtures. *Ind Eng Chem Res*. 2002;41:3326–3328.
33. Muhmood L, Viswanathan N, Iwase M, Seetharaman S. Evaluating the diffusion coefficient of sulfur in low-silica CaO-SiO_2-Al_2O_3 slag. *Metall Mater Trans B*. 2011;42:274–280.
34. Eisenhüttenleute VD, editor. Slag Atlas. Düsseldorf: Verlag Stahleisen, 1995.

Manuscript received Jan. 5, 2013.